Contents lists available at ScienceDirect

Scripta Materialia

Synthesis of Cs_2TeI_6 thin film and its NO_2 gas-sensing properties under blue-light illumination

Phung Dinh Hoat[a], Yeonghun Yun[a], ByungJin Park[a], Pham Tien Hung[b], Vu Xuan Hien[c], Joon-Hyung Lee[a,d], Sangwook Lee[a,d], Young-Woo Heo[a,d,*]

[a] School of Materials Science and Engineering, Kyungpook National University (KNU), Daegu 41566, South Korea
[b] Department of Physics, Le Quy Don Technical University, No. 236 Hoang Quoc Viet Street, Hanoi, Viet Nam
[c] School of Engineering Physics, Hanoi University of Science and Technology (HUST), No. 01 Dai Co Viet Street, Hanoi, Viet Nam
[d] KNU Advanced Material Research Institute, Kyungpook National University, Daegu 41566, South Korea

ARTICLE INFO

ABSTRACT

In this study, a thin film of Cs2TeI6 perovskite with a thickness of 1.27 mm was prepared on a glass sub-strate via a non-solution process. The characteristics of the material such as phase structure, morphology, optical absorption were studied. The gas-sensing properties of the Cs2TeI6-based sensor were investigated at 25 °C using various gases under illumination of a 450-nm laser. Under the blue-light illumination, the sensor exhibited good selectivity toward NO2 gas, with a very low limit of detection of 25 ppb and re-sponsivity of 4.4% toward 1 ppm NO2. The NO2-sensing mechanism was proposed and discussed in term of a surface depletion model. The effects of light intensity, light wavelength, humidity, and long-term du-ration on NO2-sensing performances were further studied, showing its potential for application into NO2 gas sensors at room temperature.

Recently, halide perovskites have emerged as promising materi-als in the field of solar cells besides conventional materials, such as silicon, cadmium telluride and copper indium gallium selenide [1–3]. With outstanding physical properties, they are also useful in other fields, such as light-emitting diodes [4], photosensors [5] and X-ray detectors [6]. Beyond the optoelectronics, for application of gas sensors, their potential for development is huge [7]. For exam-ples, MASnI$_3$ [8] and MAPbI$_3$ [9] can detect nitrogen dioxide (NO_2) with limit of detection of 25 ppb and 1 ppm, respectively. MAPbBr$_3$ has been studied for sensing humidity [10] and CsPbBr$_3$ for sensing acetone [11], oxygen [11], and hydrogen chloride gas [12]. However, the investigated perovskite materials for practical applications are still small, due to their instability when exposed to moisture, heat or light [13–15]. One of the effective ways to overcome their insta-bility is to develop all-inorganic perovskites with enhanced stabil-ity and long-term durability.

Cs_2TeI_6 is one such material; due to the lack of organic com-ponents, it is not easy to decompose in ambient conditions. It was also considered to have good thermodynamic stability, with high formation energy ΔH of - 0.71 eV [16], which is much higher than

that of other A_2TeI_6 or well-known perovskites as MAPbI$_3$, FAPbI$_3$. To the best of our knowledge, Cs_2TeI_6 has only been potential eval-uated for optoelectronic devices and X-ray detectors [17–19], with no published information on its gas sensor. In this study, we de-veloped a facile fabrication process for making a Cs_2TeI_6 thin film using a non-solution method, and the characteristics of a gas sen-sor based on the Cs_2TeI_6 film were investigated.

Unlike metal-oxide gas sensors which typically work at high temperatures or under UV-light illumination, this Cs_2TeI_6-based sensor can operate at room temperature (25 °C) under blue-light illumination. Thus it consumes much less energy and lowers the risk of undesired reactions of combustible gases or the influence of UV radiation on the human body.

At first, the basic properties of the Cs_2TeI_6 film were charac-terized by X-ray diffraction (XRD), scanning electron microscopy (SEM), ultraviolet-visible-near-infrared (UV-VIS-NIR) spectroscopy measurements and X-ray photoelectron spectroscopy (XPS). After that, at 25 °C, under blue-light illumination, the Cs_2TeI_6 film was investigated showing its selectivity towards NO_2 with a low limit of detection (LOD) of 25 ppb. Its NO_2-sensing properties were then studied under various working circumstances (varying light inten-sity, wavelength, humidity) and the NO_2-sensing mechanism was also proposed and discussed in order to develop this material for room-temperature NO_2 gas sensors.

* Corresponding author at: School of Materials Science and Engineering, Kyung-pook National University, 80 Daehakro, Buk-gu, Daegu 41566, South Korea.
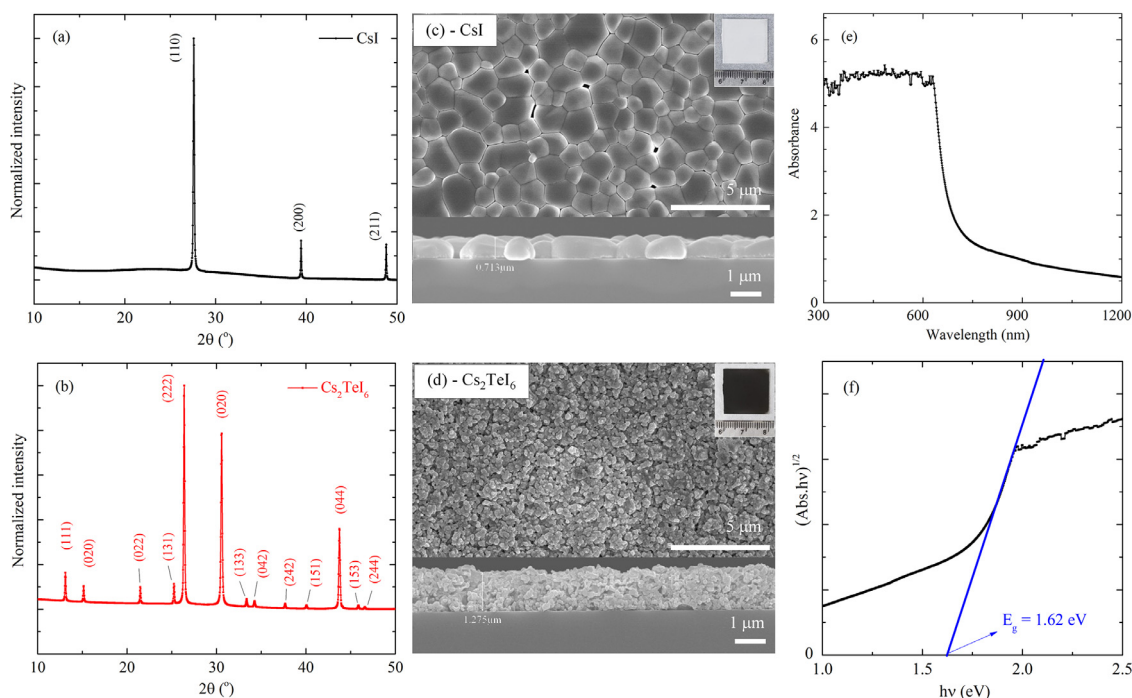*E-mail address:* ywheo@knu.ac.kr (Y.-W. Heo).

Fig. 1. (a,b) XRD patterns of CsI film after step 1 and Cs_2TeI_6 film after step 2. (c,d) Top-view and cross-sectional pictures of CsI and Cs_2TeI_6 films; the insets are photographs of CsI and Cs_2TeI_6 films on 20 × 20 mm glass substrate, respectively. (e,f) Absorbance spectra and the plot of $(abs.h\nu)^{0.5}$ versus $h\nu$ to determine energy bandgap of Cs_2TeI_6 thin film.

The synthesis of Cs_2TeI_6 involves two main steps: growth of CsI film via CVD method and annealing the CsI film in TeI_4 vapor. First, CsI powder (150 mg, 99.9%, Alfa Aesar) and the glass substrate were put into a quartz tube (Fig. S1) and maintained for 10 min at 425 and 300 °C, respectively). Argon gas was injected into the system to guarantee a working pressure of 4 Pa. Second, the CsI film and TeI_4 powder (120 mg, 99.9%, Alfa Aesar) were placed in an alumina chamber and then annealed at 210 °C for 1 h (Fig. S2). The experimental procedure of measuring properties of the film was described in detail in Supplementary Material.

XRD patterns of the films after each step are shown in Fig. 1(a-b). After Step 1, the film exhibits the cubic phase (Pm-3m) of CsI (JCPDS 01-077-2185). After Step 2, all XRD peaks can be assigned to the Cs_2TeI_6 phase; it has cubic structure (Fm-3m) (JCPDS 01-073-0330), where the major peaks at 26.37°, 30.58° and 43.74° are consistent with the corresponding (222), (020), and (044) diffraction planes. Moreover, the characteristic peaks associated with CsI, TeI_4, or other impurities are not present in the film. The formation of the Cs_2TeI_6 film may proceed:

$$2CsI_{(film)} + TeI_{4(vapor)} \rightarrow Cs_2TeI_{6(film)} \qquad (1)$$
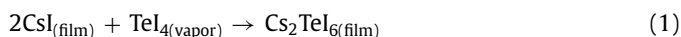
The inset images in Fig. 1(c-d) show photographs of the 20 × 20 mm CsI and Cs_2TeI_6 films, respectively. After Step 1, the film has a white color, whereas its color changes to shiny black after Step 2. The top-view images of the CsI and Cs_2TeI_6 films are shown in Fig. 1(c-d), respectively. The CsI film is made up of tightly arranged grains of $\sim$ 1–2 μm in size with clear boundaries; the Cs_2TeI_6 film is a dense, uniform and continuous film with a good adhesion to the substrate. From the XRD pattern, the Cs_2TeI_6 film is made up of 32-nm-size crystallites calculated by the Scherrer equation, $d = k\lambda/(\beta cos\theta)$, where k = 0.9, λ(Cu-Kα_1) = 1.540598 Å, at the most intense peak: θ = 13.185° and β = 4.363 × 10^{-3} rad.

The cross-sectional images (Fig. 1(c-d)) show the CsI thickness of 0.71 μm, which then increased to 1.27 μm for Cs_2TeI_6 film. The absorption spectrum of Cs_2TeI_6 film in the range of 300–1200 nm

is shown in Fig. 1e. The absorbance is quite low (around 1) in the infrared region ($\lambda \geq$ 800 nm) but rapidly increases in the visible region; especially, it becomes higher than 5 in the range of 300–630 nm. As an indirect bandgap [20–22], the optical bandgap was determined of 1.62 eV by the Tauc method (Fig. 1f); it is consistent with experimental studies showing the Cs_2TeI_6 bandgap of 1.59 [20] and 1.57 eV [19].

On the surface of Cs_2TeI_6 film, the presence of Cs, Te, I elements was demonstrated on XPS spectra (Fig. 2(a-c)). The appearance of formal Cs^+ state was indicated by two intense spin-orbit peaks at 724.5 and 738.5 eV [23-24]; while that of Te^{4+} by two peaks at 576.1, 586.4 eV [25-26] and that of I^- by two peaks at 619.0, 630.5 eV [27-28], respectively. Besides, there are minor peaks corresponding to $Te°$ and I^{5+} states at 573.7, 584.1.4 eV [29] and 623.9, 635.6 eV [27], respectively; it may be caused by: the Te-I bonding is covalent (electronegativity difference of 0.4 eV) and the charge is likely changed from formal oxidation states through covalent bonding interactions [20,30-31].

Fig. 2d showed the photoresponse of the device under 450-nm laser (32 mW/cm^2). In the dark, the Cs_2TeI_6 film has a large resistance value ($\sim$ 1.6 × 10^{11} Ω), consistent with very low conductivity in published studies [18–20]; it quickly dropped to 3.9 × 10^9 Ω under illumination. The photoresponse is a fast process with the response/recovery times of 60/100 ms. The decrease in resistance is due to the creation of large amounts of charge carriers inside the Cs_2TeI_6 film under blue-light illumination [17–19].

To evaluate the gas-sensing performance, the responses of the Cs_2TeI_6 film toward 1 ppm NO_2 were carried out in the dark and under blue-light illumination (Fig. 2e). In the dark, the resistance does not have any measurable variation when switching from dry air to NO_2 and vice versa. In contrast, under blue-light illumination, it shows a clear enhancement of NO_2 response compared to that without illumination. The resistance obviously increased in presence of NO_2 and recovered after purged out, representing the n-type semiconducting property of the Cs_2TeI_6-based device, suitable with studies [18–20]. The rise/decay times are determined of
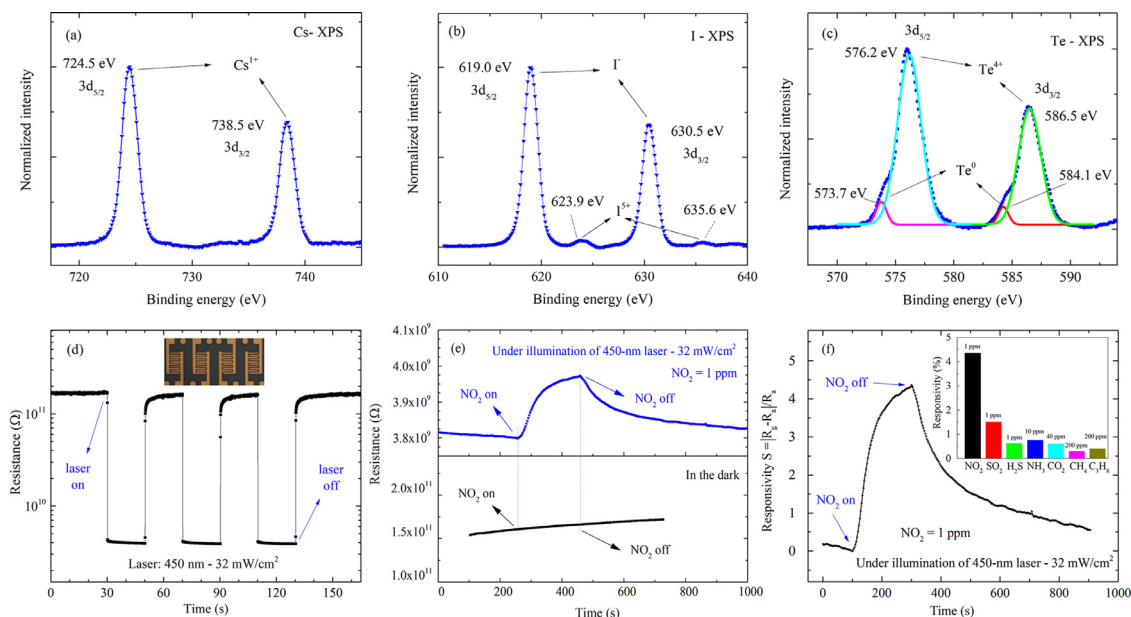
Fig. 2. (a,b,c) High-resolution X-ray photoemission spectra of Cs-3d, I-3d and Te-3d of Cs_2TeI_6 film, respectively. (d) Modulation of the device under blue-light illumination (450 nm, 32 mW/cm^2); inset is a photograph of 4 Cs_2TeI_6–based sensors on a glass substrate. (e) Responses of the Cs_2TeI_6 film toward 1 ppm NO_2 in the dark and under blue-light illumination. (f) Responsivity toward 1 ppm NO_2; inset is a comparison with other gases at different concentrations.

$\sim$ 125/600 s, respectively. These response times may be improved by using a thinner/rougher film, metal decorating/doping or applying some nanostructures/heterostructures. To examine the selectivity of the sensor, some reference gases such as SO_2, CO_2, NH_3, H_2S, CH_4 and C_3H_8 were used. In the dark, there was no appreciable change in the resistance in the presence of these gases (Fig. S3). Under blue-light illumination, Fig. 2f showed the highest responsivity of 4.36% toward 1 ppm NO_2; meanwhile, it showed much lower responsivities at similar or higher concentrations of other gases, exhibiting a good selectivity toward NO_2 of the Cs_2TeI_6-based sensor. This may be due to the different reaction energies of the test gases on the surface of the film [32].

The NO_2 response was further investigated in various concentrations from 25 ppb to 1000 ppb. In the dynamic response (Fig. 3a), the sensor can detect NO_2 at a very low concentration with LOD of 25 ppb; it is smaller than recently published values of metal-oxide gas sensors working at room temperature [33–37]. The higher the NO_2 concentration, the higher response; the responsivity increases from 0.87% for 25 ppb to 4.36% for 1000 ppb NO_2. Fig. 3b shows a linear dependence of responsivity on the log value of NO_2 concentration in this range with a linear correlation coefficient (R^2) of 0.985.

Other parameters important for gas sensors are short-term and long-term stabilities. A modulation curve toward 1 ppm NO_2 (Fig. 3c) shows that the response remains relatively stable after four on/off cycles, demonstrating favorable repeatability. Meanwhile, in Fig. 3d, the responsivity is almost unchanged for 6 weeks in ambient air (25 °C, 30–50% RH), showing the good long-term stability of the Cs_2TeI_6-based sensor.

The effect of blue-light illumination on the NO_2 response was further studied by varying intensity of the 450-nm laser. The response/recovery curves and responsivities toward 1 ppm NO_2 under different intensities were shown in Fig. 3(e-f); the dependence of resistance and responsivity on the blue-light intensity was summarized in Fig. S4. In detail, when the intensity increases from 3.2 to 10.5 and 32.0 mW/cm^2, the resistance decreases from 2.94×10^{10} to 1.06×10^{10} and 3.9×10^9 Ω, and the responsivity increases from 2.41 to 3.54 and 4.36%, respectively. The reason may be that when the light intensity is increased, the amount of photo-

electrons increases, leading to the increase not only in conductivity but also in NO_2 response [33-34, 38]. In addition, the NO_2 response was also investigated under illuminations of 520-nm (green) and 655-nm (red) lasers. Figure S5 shows that with a longer wavelength, even of greater intensity, the responsivities are still lower than that under the blue laser.

Herein, we propose the NO_2 gas-sensing mechanism of the Cs_2TeI_6 film in the dark and under blue-light illumination as illustrated in Fig. 4a. In halide perovskites, at RT, oxygen tends to adsorb electrons on the surface, similar to the metal-oxide gas-sensing semiconductors [8,39-40], it also can be adsorbed by filling into iodine vacancies ($V_I^{\cdot}$) [11,40-41]. In O-1s XPS spectrum in the air (Fig. 4b), the peak at 530.5 eV may be derived from the oxygen bonding within the lattice when oxygen fill into iodine vacancies [29,42–44]; and the peak at 532.4 eV assigned to the chemisorbed oxygen species on the surface [45]. These oxygen adsorptions led to the formation of a surface depletion layer, following the increase of its resistance when switching from N_2 ambient to dry air (Fig. S6).

In the dark:

At RT, the chemisorbed oxygen ions $O_2^{-}{}_{ads}$ are in the stable state [46–48]; so that when NO_2 is introduced into the chamber, the adsorption of NO_2 via the redox reactions may be considered to be negligible without the assistance of any external energy. It was confirmed by: When switching to NO_2, the resistance does not have any measurable variation (Fig. 2e), no change on the positions of O-1s peaks compared to these in the air (Fig. 4b) and no XPS peak of N-1s appeared (Fig. 4c).

Under illumination of blue-light 450-nm laser:

With a photoenergy (2.76 eV) larger than the bandgap of Cs_2TeI_6 (1.62 eV), a huge amount of photogenerated electrons $e^{-}{}_{h\nu}$ was created. Similar to in the dark, O_2 in the air also reacted with $e^{-}{}_{h\nu}$ to absorb on the surface [8,39-40] or fill into iodine vacancies [11,40-41], leading to the formation of photoinduced oxygen ions $O_2^{-}{}_{h\nu}$. The appearance of $O_2^{-}{}_{h\nu}$ led to higher resistance of the Cs_2TeI_6 film when changing from N_2 ambient to dry air (Fig. S6).

When exposed to NO_2, with the support of photoactivation energy of blue light, we suggest that NO_2 can be adsorbed into the
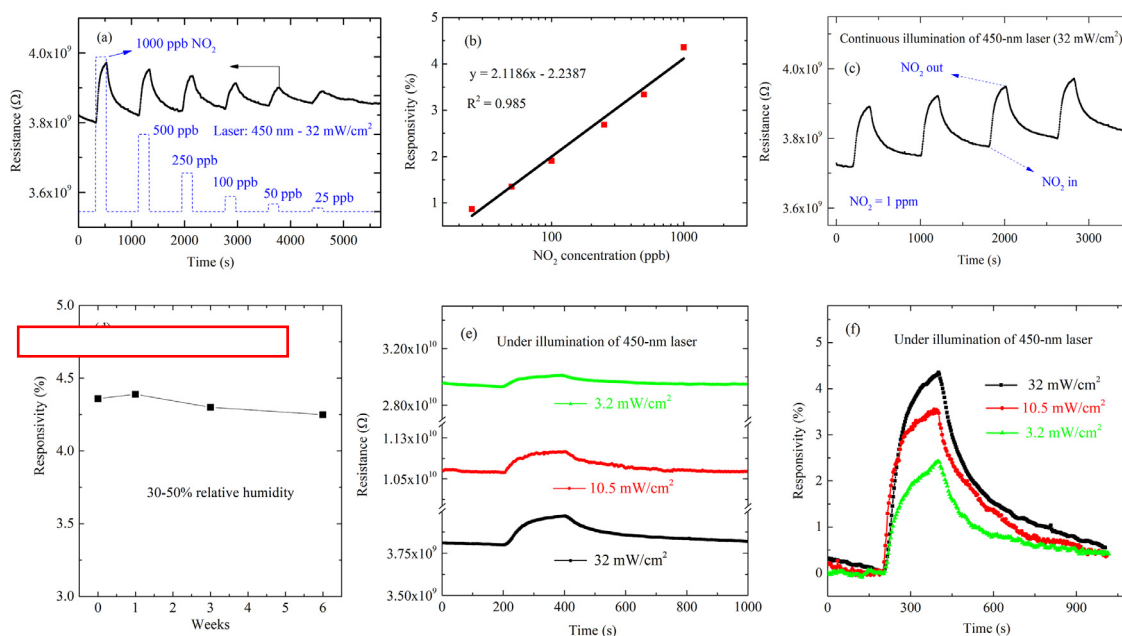
Fig. 3. (a) Dynamic response to the various concentration of NO$_2$. (b) Relationship between responsivity and NO$_2$ concentration in 25-1000 ppb range. (c) Gas-sensing modulation curve of Cs$_2$TeI$_6$ film toward 1 ppm NO$_2$ under continuous illumination of a blue laser (450 nm, 32 mW/cm^2). (d) The long-term stability of the Cs$_2$TeI$_6$ sensor in humid air (30-50%) for 6 weeks. (e,f) The response/recovery curves and responsivity toward 1 ppm NO$_2$ under the different intensities of 450-nm laser illumination.
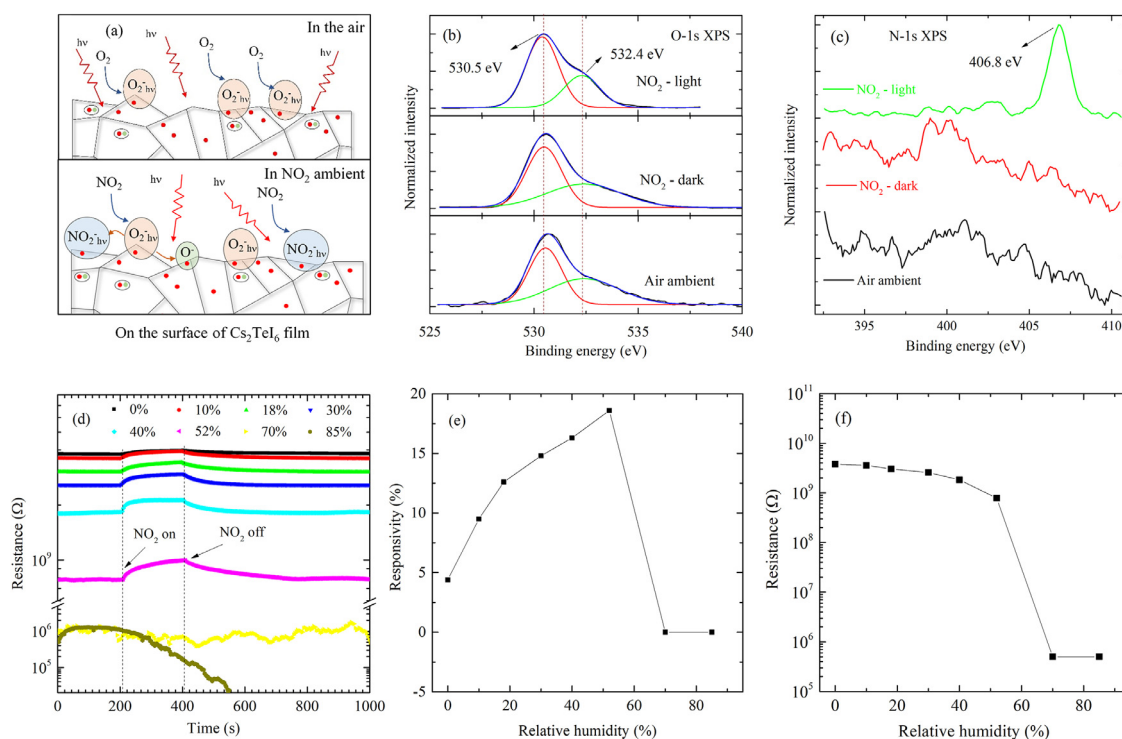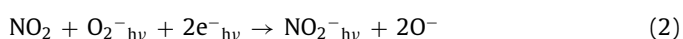

Fig. 4. (a) Schematic illustration of the possible NO$_2$-sensing mechanism of Cs$_2$TeI$_6$-based sensor under blue-light illumination. (b,c) The XPS spectra of O-1s and N-1s of Cs$_2$TeI$_6$ film in air ambient and when exposured to NO$_2$. (d,e,f) The effect of humidity on resistance and responsivity toward 1 ppm NO$_2$ of the Cs$_2$TeI$_6$ film at 25 °C under blue-light illumination (450 nm, 32 mW/cm^2).

Cs$_2$TeI$_6$ film via the well-known redox reaction with $e^-_{h\nu}$ and $O_2^-{}_{h\nu}$ as followed [33,36,45,49]:

$$NO_2 + O_2^-{}_{h\nu} + 2e^-_{h\nu} \rightarrow NO_2^-{}_{h\nu} + 2O^- \quad (2)$$

$$NO_2 + e^-_{h\nu} \rightarrow NO_2^-{}_{h\nu} \quad (3)$$

The NO$_2$ adsorptions under blue-light illumination was confirmed by XPS measurement that: When exposed to NO$_2$ gas, there

was an appearance of N-1s peak at 406.8 eV compared to that without NO$_2$ (Fig. 4c). The NO$_2$ adsorptions increased the width of the depletion layer in the presence of NO$_2$, increasing the resistance of the Cs$_2$TeI$_6$ film (Fig. 2e). When NO$_2$ was purged out of the chamber, Reactions (2-3) proceed in the opposite direction meaning recovery of the resistance.

One of the most important factors to consider for a gas sensor operating at RT is humidity. The effect of 0–85% RH on the response toward 1 ppm NO$_2$ was investigated under 450-nm laser

(32 mW/cm^2) and summarized in Fig. 4(d-f) with the following observations:

- With the increase of humidity, the base resistance gradually decreases from 3.9×10^9 Ω at 0% RH to 7.8×10^8 Ω at 52% RH and then rapidly decreases to $\sim 10^5$ Ω at 70% RH or higher. It is because adsorbed water causes an enhancement in conductivity via e$^-$ injection due to the formation of hydroxyl radicals [50], which in turn reduces the resistance of the device. At high RH ($\geq$ 70%), a continuous water layer is formed on the surface, promoting bulk conduction between electrodes [50], so that when RH increases from 70% to 85%, no further change of resistance is observed (Fig. 4d). An additional test at 70% RH was made to examine the change in resistance upon switching the light off. In Fig. S7, no change in resistance confirms that the electrical current flows through the absorbed water layer but instead the Cs$_2$TeI$_6$ film.

- Responsivity increases to 18.3% when the RH increases to 52%, but quickly drops to zero at high RH ($\geq$ 70%). It can be explained that: At low RH region, when increasing RH, the electron injection supplies more e$^-$ (and O$_2^-$ ions) on the surface, following the enhancement of NO$_2$ response. However, at high RH ($\geq$ 70%), the coverage of the physisorbed water layer blocks the adsorption sites [28,34,51], leading to a huge decrease of NO$_2$ response. To determine if the humid air reacts with the film, another Cs$_2$TeI$_6$ sample was placed under a 70%-RH flow for 4 h; XRD pattern (Fig. S8) indicated that water molecules are only adsorbed on the surface, without causing any phase change of the Cs$_2$TeI$_6$ film.

In this work, a thin film of Cs$_2$TeI$_6$ was synthesized using a non-solution method via two processes: the fabrication of a CsI film via CVD and annealing the CsI film in TeI$_4$ vapor. Some basic properties of Cs$_2$TeI$_6$ film were studied to provide useful data for further research. Under blue-light illumination, the Cs$_2$TeI$_6$ film acts as a NO$_2$ gas-sensing material at 25 °C, showing a responsivity of 4.4% toward 1 ppm NO$_2$ and LOD of 25 ppb. The effects of humidity and long duration on the NO$_2$ response were also investigated, showing the maximum responsivity of 18.3% at 52% RH and the long-term stability of 6 weeks. All results indicate that Cs$_2$TeI$_6$ is a promising material using for NO$_2$ gas sensors at RT.

Declaration of Competing Interest

On behalf of all authors of the manuscript entitled "**Synthesis of Cs$_2$TeI$_6$ thin film and its NO$_2$ gas-sensing properties under blue-light illumination**", I certify that there is no conflict of interest with any financial organization regarding the material discussed in the manuscript.

Acknowledgments

Supplementary materials

Supplementary material associated with this article can be found, in the online version, at doi:10.1016/j.scriptamat.2021.114305.

References

[1] C. Liu, D. Chen, Y. Chen, Y. Ling, Y. Zou, Y. Wang, J. Gong, Z. Feng, P.P. Altermatt, P.J. Verlinden, Sol. Energy Mater. Sol. Cells 215 (2020) 1–5.
[2] G. Kartopu, B.L. Williams, V. Zardetto, A.K. Gurlek, A.J. Clayton, S. Jones, W.M.M. Kessels, M. Creatore, S.J.C. Irvine, Sol. Energy Mater. Sol. Cells 191 (2019) 78–82.
[3] S.R.F.S. Panahi, A. Abbasi, V. Ghods, M. Amirahmadi, J. Mater. Sci. Mater. Electron. 31 (2020).
[4] L. Zhang, L. Xu, M. Zhu, C. Li, L. Li, J. Su, Y. Gao, J. Alloys Compd. 818 (2020) 152913.
[5] Y. Wang, Y. Zhang, T. Pang, K. Sun, Z. Hu, Y. Zhu, R. Jia, Sol. Energy 183 (2019) 226–233.
[6] X. Zheng, W. Zhao, P. Wang, H. Tan, M.I. Saidaminov, J. Energy Chem. 49 (2020) 299–306.
[7] Z. Zhu, Q. Sun, Z. Zhang, J. Dai, G. Xing, S. Li, X. Huang, W. Huang, J. Mater. Chem. C 6 (2018) 10121–10137.
[8] V.X. Hien, P.T. Hung, J. Han, S. Lee, J.H. Lee, Y.W. Heo, Scr. Mater. 178 (2020) 108–113.
[9] X. Fu, S. Jiao, N. Dong, G. Lian, T. Zhao, S. Lv, Q. Wang, D. Cui, RSC Adv. 8 (2018) 390–395.
[10] W. Xu, F. Li, Z. Cai, Y. Wang, F. Luo, X. Chen, J. Mater. Chem. C 4 (2016) 9651–9655.
[11] H. Chen, M. Zhang, R. Bo, C. Barugkin, L. Zhang, Q. Ma, S. Huang, A.W.Y. Ho-Baillie, K.R. Catchpole, A. Tricoli, Small 14 (2018) 1–7.
[12] X. Chen, H. Hu, Z. Xia, W. Gao, W. Gou, Y. Qu, Y. Ma, J. Mater. Chem. C 5 (2017) 309–313.
[13] T. Leijtens, G.E. Eperon, N.K. Noel, S.N. Habisreutinger, A. Petrozza, H.J. Snaith, Adv. Energy Mater. 5 (2015) 1500963.
[14] N. Aristidou, I. Sanchez-Molina, T. Chotchuandchutchaval, M. Brown, L. Martinez, T. Rath, S.A. Haque, Angew. Chemie - Int. Ed. 54 (2015) 8208–8212.
[15] Y. Zhou, Y. Zhao, Energy Environ. Sci. 12 (2019) 1495–1511.
[16] D. Liu, Q. Li, Z. Zhang, K. Wu, New J. Chem. 43 (2019) 14892–14897.
[17] I. Vázquez-Fernández, S. Mariotti, O.S. Hutter, M. Birkett, T.D. Veal, T.D.C. Hobson, L.J. Phillips, L. Danos, P.K. nayak, H.J. Snaith, W. Xie, M.P. Sherburne, M. Asta, K. Durose, Chem. Mater. 32 (2020) 6676–6684.
[18] J. Guo, W.Yang Y.Xu, B. Zang, J. Dong, W. Jie, M.G. kanatzidis, J. Mater. Chem. C 7 (2019) 8712–8719.
[19] Y. Xu, B. Jiao, T. Song, C.C. Stoumpos, Y. He, I. Hadar, W. Lin, W. Jie, M.G. Kanatzidis, ACS Photonics 6 (2019) 196–203.
[20] A.E. Maughan, A.M. Ganose, M.M. Bordelon, E.M. Miller, D.O. Scanlon, J.R. Neilson, J. Am. Chem. Soc. 138 (2016) 8453–8464.
[21] Y. Cai, W. Xie, H. Ding, Y. Chen, K. Thirumal, L.H. Wong, N. Mathews, S.G. Mahaisalkar, M. Sherburne, M. Asta, Chem. Mater. 29 (2017) 7740–7749.
[22] E.Y. Peresh, O.V. Zubaka, V.I. Sidei, I.E. Barchii, S.V. Kun, A.V. Kun, Inorganic Mater. 38 (2002) 859–863.
[23] P.D. Hoat, H.H. Ha, P.T. Hung, V.X. Hien, S. Lee, J. Lee, Y. Heo, Thin Solid Films 732 (2021) 138799.
[24] L. Dimesso, C. Das, M. Stöhr, T. Mayer, W. Jaegermann, Mater. Chem. Phys. 197 (2017) 27–35.
[25] A. Mekki, G.D. Khattak, L.E. Wenger, J. Non. Cryst. Solids 352 (2006) 3326–3331.
[26] S. Tari, F. Aqariden, Y. Chang, C. Grein, J. Li, N. Kioussis, J. Electron. Mater. 42 (2013) 3252–3258.
[27] K. Li, Y. Zhao, C.He P.Zhang, J. Deng, S. Ding, Appl. Surf. Sci. 390 (2016) 412–421.
[28] Y. Chen, X. Zhang, Z. Liu, Z. Zeng, H. Zhao, X. Wang, J. Xu, Microchimica Acta 186 (2019).
[29] A.B. Nedelcheva, R. Iordanova, K.L. Kostov, Mater. Res. Express 6 (2019) 125202.
[30] G. Aullón, S. Alvarez, Theor. Chem. Acc. 123 (2009) 67–73.
[31] M. Jansen, U. Wedig, Angew. Chemie - Int. Ed., 47 (2008) 10026–10029.
[32] S.T. Navale, A.T. Mane, M.A. Chougule, R.D. Sakhare, S.R. Nalage, V.B. Patil, Synth. Met. 189 (2014) 94–99.
[33] C. Zhang, A. Boudiba, P. De Marco, R. Snyders, M.G. Olivier, M. Debliquy, Sens. Actuat. B Chem. 181 (2013) 395–401.
[34] N.M. Hung, N.M. Hieu, N.D. Chinh, T.T. Hien, N.D. Quang, S. Majumder, G. Choi, C. Kim, D. Kim, Sens. Actuat., B Chem. 313 (2020) 128001.
[35] T. Xie, N. Sullivan, K. Steffens, B. Wen, G. Liu, R. Debnath, A. Davydov, R. Gomez, A. Motayed, J. Alloys Compd. 653 (2015) 255–259.
[36] F.H. Saboor, T. Ueda, K. Kamada, T. Hyodo, Y. Mortazavi, A.A. Khodadadi, Y. Shimizu, Sens. Actuat. B Chem. 223 (2016) 429–439.
[37] Y. Mun, S. Park, S. An, C. Lee, H.W. Kim, Ceram. Int. 39 (2013) 8615–8622.
[38] X. Geng, C. Zhang, M. Debliquy, Ceram. Int. 42 (2016) 4845–4852.
[39] F. Wang, J. Ma, F. Xie, L. Li, J. Chen, J. Fan, N. Zhao, Adv. Funct. Mater. 26 (2016) 3417–3423.
[40] M.A. Stoeckel, M. Gobbi. S. Bonacchi, L.Ferlauto F.Liscio, E. Orgiu, P. Samori, Adv. Mater. 29 (2017) 1702469.
[41] N. Aristidou, C. Eames, I.S. Molina, X. Bu, J. Kosco, M.S. Islam, S.A. Haque, Nat. Commun. 8 (2017) 1–10.
[42] B.V.R. Chowdari, P.Pramoda Kumari, J. Non. Cryst. Solids 197 (1996) 31–40.
[43] P. Charton, L. Gengembre, P. Armand, J. Solid State Chem. 168 (2002) 175–183.
[44] M.T. Rinke, L. Zhang, H. Eckert, Chem. Phys. Chem. 8 (2007) 1988–1998.
[45] D. Gu, X. Wang, W. Liu, X. Li, S. Lin, J. Wang, M.N. Rumyantseva, A.M. Gaskow, S.A. Akbar, Sens. Actuat. B Chem. 305 (2020) 127455.
[46] Sunghoon Park, S. An, Y. Mun, C. Lee, Appl. Mater. Interfaces 5 (2013) 4285–4292.
[47] X. Li, X. Li, J. Wang, S. Lin, Sens. Actuat. B Chem 219 (2015) 158–163.
[48] E. Zampetti, A. Macagnano, A. Bearzotti, J. Nanopart. Res. 15 (2013) 1566–1569.
[49] V.X. Hien, Y.W. Heo, Sens. Actuat. B Chem 228 (2016) 185–191.
[50] G. Volp, V.H. Grassian, Chem. Commun. 49 (2013) 3071–3094.
[51] D.S. Vlachos, P.D. Skafidas, J.N. Avaritsiotis, Sens. Actuat.: B. Chem. 25 (1995) 491–494.